Seismic anisotropy beneath the Afar Depression and adjacent areas: Implications for mantle flow

Stephen S. Gao,[1] Kelly H. Liu,[1] and Mohamed G. Abdelsalam[1]

Received 17 November 2009; revised 14 September 2010; accepted 27 September 2010; published 30 December 2010.

[1] Shear wave splitting is a robust tool to infer the direction and strength of seismic anisotropy in the lithosphere and underlying asthenosphere. Previous shear wave splitting studies in the Afar Depression and adjacent areas concluded that either Precambrian sutures or vertical magmatic dikes are mostly responsible for the observed anisotropy. Here we report results of a systematic analysis of teleseismic shear wave splitting using all the available broadband seismic data recorded in the Afar Depression, Main Ethiopian Rift (MER), and Ethiopian Plateau. We found that while the ~450 measurements on the Ethiopian Plateau and in the MER show insignificant azimuthal variations with MER-parallel fast directions and thus can be explained by a single layer of anisotropy, the ~150 measurements in the Afar Depression reveal a systematic azimuthal dependence of splitting parameters with a $\pi/2$ periodicity, suggesting a two-layer model of anisotropy. The top layer is characterized by a relatively small (0.65 s) splitting delay time and a WNW fast direction that can be attributed to magmatic dikes within the lithosphere, and the lower layer has a larger (2.0 s) delay time and a NE fast direction. Using the spatial coherency of the splitting parameters obtained in the MER and on the Ethiopian Plateau, we estimated that the optimal depth of the source of anisotropy is centered at about 300 km, i.e., in the asthenosphere. The spatial and azimuthal variations of the observed anisotropy can best be explained by a NE directed flow in the asthenosphere beneath the MER and the Afar Depression.

Citation: Gao, S. S., K. H. Liu, and M. G. Abdelsalam (2010), Seismic anisotropy beneath the Afar Depression and adjacent areas: Implications for mantle flow, *J. Geophys. Res.*, *115*, B12330, doi:10.1029/2009JB007141.

1. Introduction

[2] Splitting of *P*-to-*S* converted phases at the core-mantle boundary (*XKS*, including *SKS*, *PKS*, and *SKKS*) is a direct manifestation of seismic anisotropy, which is mostly the result of deformational processes in the Earth's lithosphere and asthenosphere. As demonstrated by hundreds of *XKS* splitting studies (see *Savage* [1999], *Fouch and Rondenay* [2006], and *Long and Silver* [2009] for reviews), spatial distribution of the two splitting parameters (ϕ, which is the polarization direction of the fast shear wave, and δt which is the splitting delay time between the fast and slow shear waves) has played an essential role in the investigation of the anisotropic structure and associated mantle dynamic processes of the Earth.

[3] The fast direction is a measure of the orientation of the anisotropy, and the splitting delay time is proportional to the product of the thickness of the anisotropic layer and the coefficient of anisotropy, which is defined as $(V_{fast} - V_{slow})/V_{mean}$ [*Birch*, 1960]. The global average of the splitting delay time obtained using teleseismic *XKS* waves is 1.0 s [*Silver*, 1996], corresponding to a thickness of about 100 km for a 4% anisotropy, when an upper mantle average shear wave velocity of 4.0 km/s is used. Mineral physics experiments and numerical modeling [e.g., *Nicolas and Christensen*, 1987; *Zhang and Karato*, 1995; *Ben Ismail and Mainprice*, 1998] suggest that in the upper mantle, seismic anisotropy measured by shear wave splitting is controlled by the alignment of the *a* axis of olivine along the flow direction through dislocation creep. In areas undergoing lithospheric shortening, the fast directions are mostly parallel to the strike of the orogenic belts, as observed in northern Tibet [*McNamara et al.*, 1994], Tienshan [*Li and Chen*, 2006], and the Ouachita orogenic belt in the southern United States [*Gao et al.*, 2008]. Vertical magmatic dikes in the lithosphere can also lead to *XKS* splitting with a fast direction parallel to the dominant strike direction of the dikes. This mechanism was proposed to explain rift-parallel fast directions observed in active continental rifts such as the Baikal Rift Zone [*Gao et al.*, 1997] and the East African Rift System (EARS) [*Gao et al.*, 1997; *Kendall et al.*, 2005] and failed rifts such as the southern Oklahoma aulacogen [*Gao et al.*, 2008]. As detailed below, mostly due to the multiple causes of shear wave splitting discussed above and the intrinsic low vertical resolution of *XKS* splitting measurements, contrasting models have been proposed to explain the

[1]Department of Geological Sciences and Engineering, Missouri University of Science and Technology, Rolla, Missouri, USA.

0148-0227/10/2009JB007141

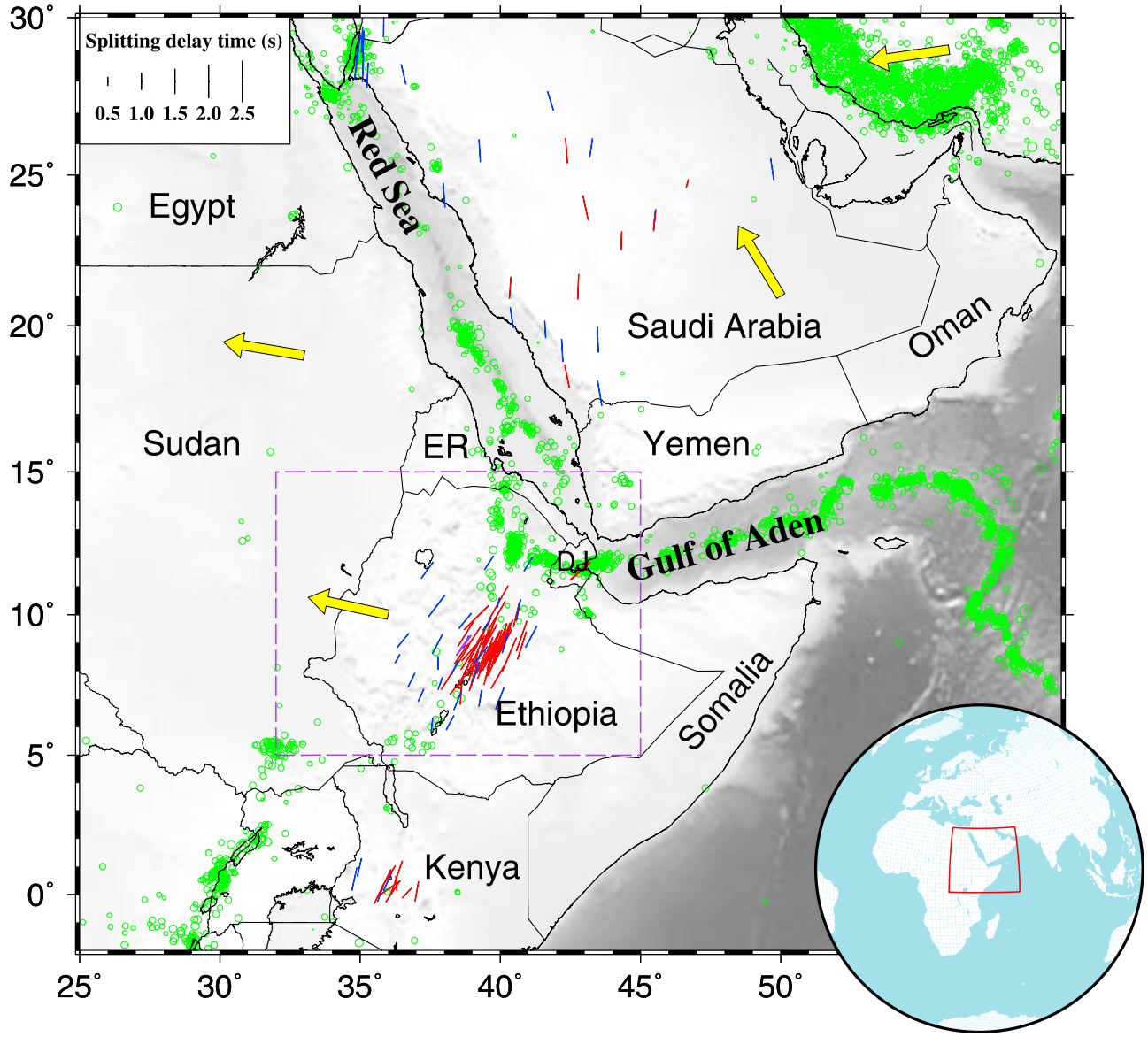

Figure 1. Map of northeastern Africa showing epicenters of magnitude 4 and greater earthquakes that have occurred since 1961 (green circles), absolute plate motion directions (yellow arrows) [*Gripp and Gordon*, 2002], and previous shear wave splitting measurements (red or blue bars). The orientation of the bars represents the fast direction, and the length is proportional to the splitting delay time. Red bars in Kenya represent measurements from *Gao et al.* [1997], and blue bars are those from *Walker et al.* [2004]. In Ethiopia, red bars are measurements from *Kendall et al.* [2005] and blue bars are those from *Gashawbeza et al.* [2004]. The measurement in Djibouti was reported by *Vinnik et al.* [1989] and *Barruol and Hoffmann* [1999]. Red bars in Saudi Arabia are measurements of *Wolfe et al.* [1999], and blue bars are from *Hansen et al.* [2006]. ER, Eritrea; DJ, Djibouti. The area inside the purple dashed rectangle is shown in Figure 2. The inset shows a hemisphere of the Earth and the location of the mapped area.

spatial distribution of shear wave splitting parameters in the vicinity of the EARS especially in the Afar Depression and its surrounding areas (Figure 1).

[4] The Afar Depression is the most developed section of the EARS. It occupies an ~200,000 km^2 area in eastern Ethiopia, Djibouti, and southeastern Eritrea (Figures 1 and 2) [*Beyene and Abdelsalam*, 2005]. The evolution of the Afar triple junction started with outpouring of flood basalt at 29 Ma (Figure 2), signaling the arrival of a mantle plume at the base of the Precambrian Arabian-Nubian Shield [*Hoffmann et al.*, 1997]. On a global scale, the Main Ethiopian Rift (MER), the Red Sea, and the Gulf of Aden join in Afar to form a classic rift-rift-rift triple junction. These three structures separate the Arabian, Nubian and Somalian plates (Figure 2). On a local scale, however, the three rifts do not meet at a single point. Instead, the Gulf of Aden steps onto the Afar Depression and propagates northwest to form the Gulf of Aden propagator, and the Red Sea steps onto Afar and propagates southeast to form the Red Sea propagator (Figure 2) [*Acocella et al.*, 2008]. These propagators are

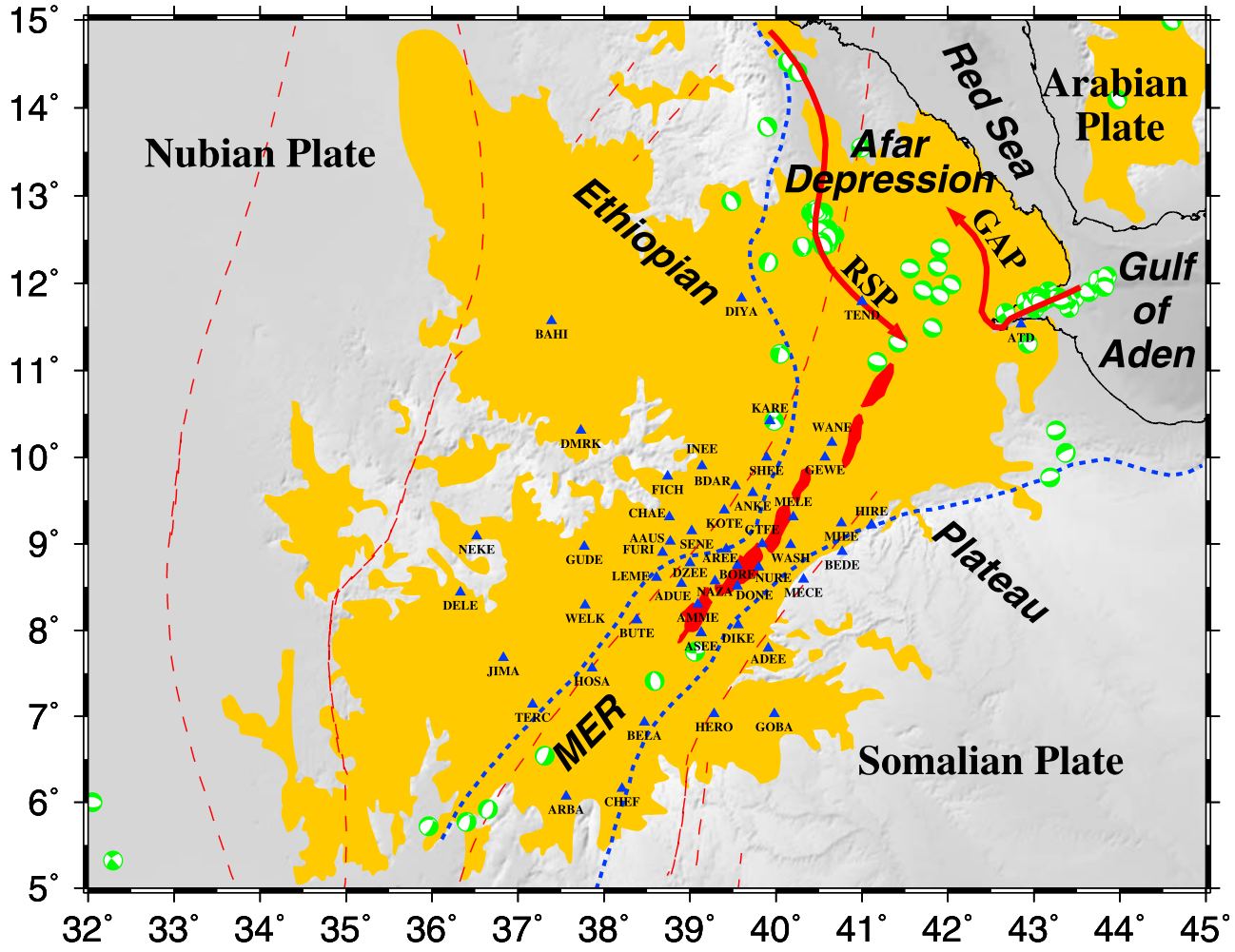

Figure 2. Topographic map of the study area showing major tectonic provinces and seismic stations (triangles) used in the study. MER, Main Ethiopian rift; RSP, Red Sea propagator; GAP, Gulf of Aden propagator. Also shown are focal mechanism solutions (green symbols) of all the earthquakes (from early 1976 to late 2009) in the Global Centroid Moment Tensor Project database (http://www.globalcmt.org), magmatic segments (filled red areas along the MER) [*Ebinger and Casey*, 2001], and distribution of flood basalts (orange area) [*Coffin and Eldholm*, 1994]. The thick dotted lines are boundaries of the rifted areas (MER and Afar), and the thin dashed lines are Precambrian sutures [*Berhe*, 1990; *Abdelsalam and Stern*, 1996].

seismically and magmatically active as exemplified by the September 2005 volcanoseismic crisis event, during which an approximately 60 km long, NW trending magmatic dike was emplaced in the northern part of the Red Sea propagator following a series of earthquakes [*Wright et al.*, 2006; *Ayele et al.*, 2007]. Such diking events have been taken to reinforce the "magma-assisted rifting" model which was first proposed for the MER to advocate for the transfer of strain from rift border faults to rift axis due to dike emplacement [*Ebinger and Casey*, 2001].

[5] Over the past 15 years *XKS* splitting studies have played an important role in providing constraints on various models for the formation, structure, and dynamics of the EARS. Based on data from 17 stations located in the axial zone of the EARS in Kenya, *Gao et al.* [1997] suggested that the dominantly rift-parallel fast directions reflect along-strike vertical magmatic dikes. Similarly, *Walker et al.* [2004] and *Kendall et al.* [2005, 2006] concluded from measurements in the northern part of the EARS including the MER that rift-parallel fast directions are due to NE elongated magmatic segments (Figure 2), supporting the magma-assisted rifting model of *Ebinger and Casey* [2001]. In contrast, *Gashawbeza et al.* [2004] revealed that the majority of the fast directions observed at 26 stations across Ethiopia are mostly subparallel to Neoproterozoic sutures (Figure 2) [*Berhe*, 1990; *Abdelsalam and Stern*, 1996], and consequently proposed that upper mantle anisotropy beneath Ethiopia is mostly the result of fossil fabrics in the lithosphere and that the MER was developed along old zones of weakness. On the basis that the Ethiopian Plateau and the Afar Depression are underlain by a slower than normal lower crustal and upper mantle shear wave velocity, *Keranen et al.* [2009] reinterpreted the results of *Gashawbeza et al.* [2004] as mostly originating from aligned melt-filled cracks.

[6] Previous shear wave splitting studies conducted in Afar and adjacent areas [*Vinnik et al.*, 1989; *Gao et al.*, 1997;

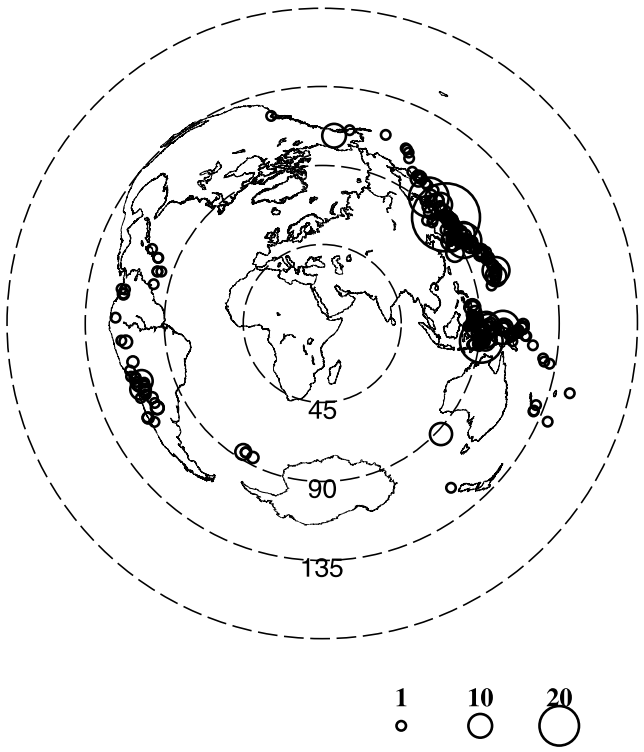

Figure 3. An azimuthal equidistant projection map of the Earth showing the distribution of earthquakes used in the study (open dots). The radius of the dots is proportional to the number of resulting well-defined splitting measurements from the events. Dashed circles and corresponding labels show the distance (in degree) to the center of the study area.

Barruol and Hoffmann, 1999; *Barruol and Ben Ismail*, 2001; *Gashawbeza et al.*, 2004; *Walker et al.*, 2004; *Kendall et al.*, 2005, 2006] used a subset of the seismic data recorded in the study area, resulting in a limited spatial coverage. Also, almost all the results from those studies were presented in the form of station-averaged splitting parameters. Such practice assumes a single layer of anisotropy with a horizontal axis of symmetry and is thus not suitable for characterizing more complicated situations such as multiple layers of anisotropy, which causes variations of the observed splitting parameters with the back azimuth (BAZ) of the events [*Silver and Savage*, 1994]. Obviously, for areas with complex anisotropy, mean splitting parameters are heavily biased toward the most populous event groups and thus may not be representative of the actual anisotropic property. In addition, like the vast majority of *XKS* splitting studies, previous studies in the EARS were unable to obtain a reliable estimate of the depth of the source of the observed anisotropy. Those factors led to contrasting geodynamic implications of the *XKS* splitting measurements.

[7] In this study we explore the existence of complex anisotropy by using all the available broadband seismic data recorded in the study area (Figure 2) and propose a procedure to estimate the depth of the source of anisotropy by measuring the spatial coherency of the splitting parameters. We conclude that the most likely origin of the observed seismic anisotropy is a NE directed asthenospheric flow beneath the MER and the Afar Depression.

2. Data and Method

[8] This study uses all the broadband *XKS* data recorded in Ethiopia and Djibouti archived at the Incorporated Research Institutions for Seismology (IRIS) Data Management Center (DMC). We choose seismic events based on the following criteria: For *PKS*, the epicentral distance range is 120–180°, and the cutoff magnitude is 5.8; for *SKKS*, the corresponding values are 95–180° and 5.6; and for *SKS*, they are 84–180° and 5.6. For events with a focal depth of 100 km or greater, the cutoff magnitude is reduced by 0.1 unit to take advantage of the sharp waveforms for all the *PKS*, *SKKS*, and *SKS* phases. Figure 3 shows the distribution of the 256 events that produced at least one well-defined measurement. The majority of the events are from the western Pacific and South American subduction zones. Relative to most previous shear wave splitting studies, the azimuthal coverage of the events is outstanding, allowing a reliable detection of complex anisotropy. Note that although data from events with epicentral distance up to 180° were requested from the IRIS DMC to avoid missing any good events, all the events with reliable *XKS* measurements have an epicentral distance range of 85.4–145.3° (Figure 3; see also Data Set S1).[1] Additionally, the 0.1 magnitude unit reduction (which represents an ~30% reduction in energy release) for deeper earthquakes only resulted in 3 additional measurements out of a total of 597 (Data Set S1), suggesting that a further reduction in the cutoff magnitude will unlikely lead to any additional measurements.

[9] Fifty-two stations were found to produce at least one well-defined *XKS* splitting measurement. Two of the stations, ATD in Djibouti and FURI at Addis Ababa, Ethiopia, belong to the GEOSCOPE and Global Seismographic Network, respectively, and the rest of the stations are from the Ethiopian Broadband Seismic Experiment (EBSE) [*Nyblade and Langston*, 2002] and the Ethiopian Afar Geophysical Lithospheric Experiment (EAGLE) [*Maguire et al.*, 2003]. A procedure for measuring and objectively ranking *XKS* splitting parameters [*Liu et al.*, 2008; *Gao and Liu*, 2009; *Liu*, 2009] based on the minimization of transverse energy method [*Silver and Chan*, 1991] was applied to the data sets. In this procedure the seismograms were band-pass filtered in the 0.04–0.5 Hz range which we found is the most effective frequency band for enhancing the signal-to-noise ratio (*S*/*N*), and the optimal *XKS* time window used is visually verified and adjusted if necessary to exclude non-*XKS* arrivals. The uncertainties in the measurements are calculated using the inverse *F* test and represent approximately 2 standard deviations [*Silver and Chan*, 1991]. Figures 4–6 show examples of the original and corrected waveforms and their particle motion diagrams.

[10] Using the procedure proposed by *Liu et al.* [2008], we quantify the quality of resulting measurements using the *S*/*N* on the original radial (R_{or}), original transverse (R_{ot}), and corrected transverse (R_{ct}) components. For a quality A measurement, $R_{or} \geq 10.0$, $R_{ot} \geq 2.0$, and $R_{ct}/R_{ot} \leq 0.7$, that is, outstanding energy on both the radial and transverse components is observed, and the resulting parameters were effective in reducing the energy on the transverse component.

[1] Auxiliary materials are available at ftp://ftp.agu.org/apend/jb/2009jb007141.

The criteria for a quality B measurement include $3.0 \leq R_{or} < 10.0$, $R_{ot} \geq 2.0$, and $R_{cf}/R_{ot} \leq 0.7$. The ranking was visually verified and adjusted if necessary.

3. Results

[11] A total of 597 well-defined (quality A and B) measurements were obtained, among which 5 are *PKS*, 30 are *SKKS*, and 562 are *SKS* measurements (Figure 7; see Data Set S1 for the measurements and additional information). The mean splitting delay time over all the 597 measurements is 1.46 ± 0.39 s, which is significantly greater than the global average of 1.0 s for continents, and corresponds to a 110–200 km thick layer with 4% anisotropy, or a 160–275 km layer with 3% anisotropy.

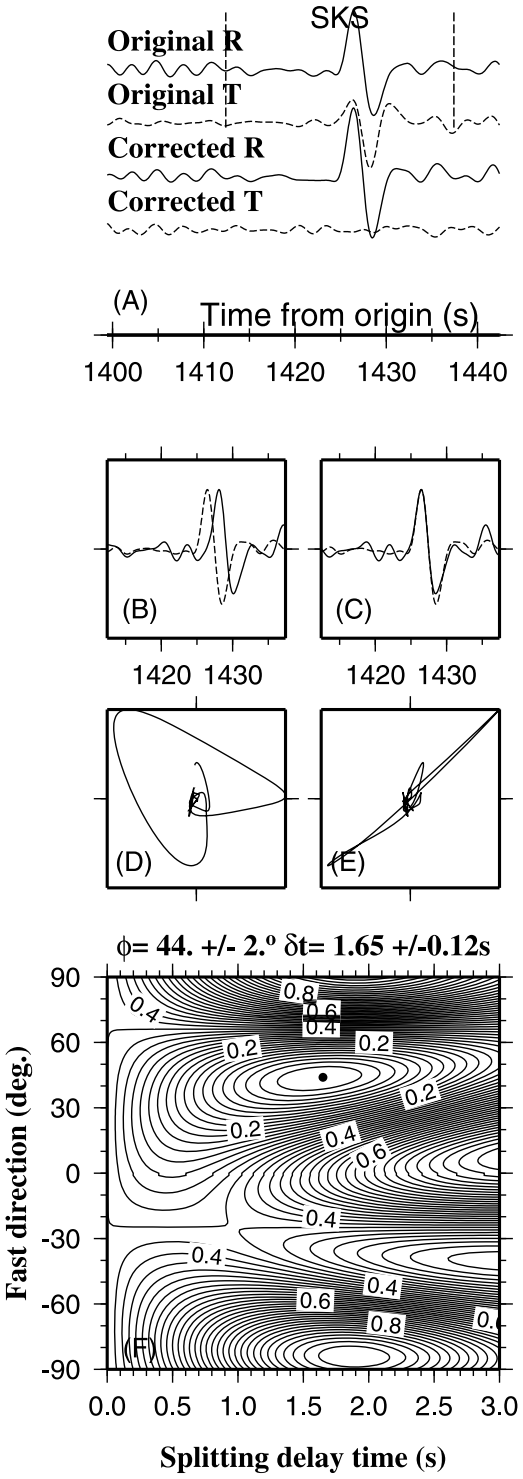

Figure 4. Diagrams associated with shear wave splitting analysis for an *SKS* phase from the ENE recorded by station ATD in the Afar Depression. (a) Original and corrected radial and transverse *XKS* arrivals. The vertical bars mark the *XKS* window used for analysis. (b) Normalized fast (dashed line) and slow (solid line) *XKS* arrivals computed using the optimal pair of splitting parameters. (c) Same as Figure 4b but the slow component was advanced by δt seconds. (d) Particle motion pattern of the normalized fast and slow arrivals shown in Figure 4b. (e) Particle motion pattern of the arrivals shown in Figure 4c. (f) Contour map of normalized energy on the corrected transverse component plotted as a function of trial ϕ and δt pairs. The optimal pair of splitting parameters is marked by the solid dot. A well-defined pair of splitting parameters is characterized by a strong *XKS* arrival on both the original radial and transverse components and a significant reduction of *XKS* energy on the corrected transverse component (Figure 4a), a high-level similarity between the waveforms of the computed fast and slow components (Figures 4b and 4c), an elliptical particle motion pattern resulted from the fast and slow components (Figure 4d), a linear particle motion from the overlapped fast and slow components (Figure 4e), and a well-defined single minimum on the energy contour (Figure 4f).

3.1. Azimuthal Dependence of Splitting Parameters

[12] The 448 measurements in the MER and on the Ethiopian Plateau show azimuthally invariable splitting parameters (Figure 8), with a mean splitting delay time of 1.44 ± 0.39 s and a mean fast direction of 25 ± 12°, which is subparallel to the surface expression of the MER (about 35°). The insignificant azimuthal variations of the splitting parameters (Figure 8) imply a single layer of anisotropy or multiple layers with similar or orthogonal fast directions, suggesting that station-averaged splitting parameters reported by previous studies [*Barruol and Hoffmann*, 1999; *Barruol and Ben Ismail*, 2001; *Gashawbeza et al.*, 2004; *Kendall et al.*, 2005, 2006] are representative of the anisotropic structure beneath the stations.

[13] In contrast, the 149 measurements from the two stations in the Afar Depression (ATD and TEND) demonstrate a previously unrecognized systematic azimuthal dependence with a period of $\pi/2$ (Figure 9), suggesting the existence of two layers of anisotropy with a horizontal axis of symmetry [*Silver and Savage*, 1994]. Examples of events from different azimuths can be found in Figures 4–6. The mean splitting delay time over the 117 measurements at ATD is 1.60 ± 0.37 s which is similar to the values obtained by *Vinnik et al.* [1989], *Barruol and Hoffmann* [1999], and *Barruol and Ben Ismail* [2001]. As summarized by *Kendall et al.* [2006], previous studies found little azimuthal variations of splitting parameters at permanent seismic stations in the entire African

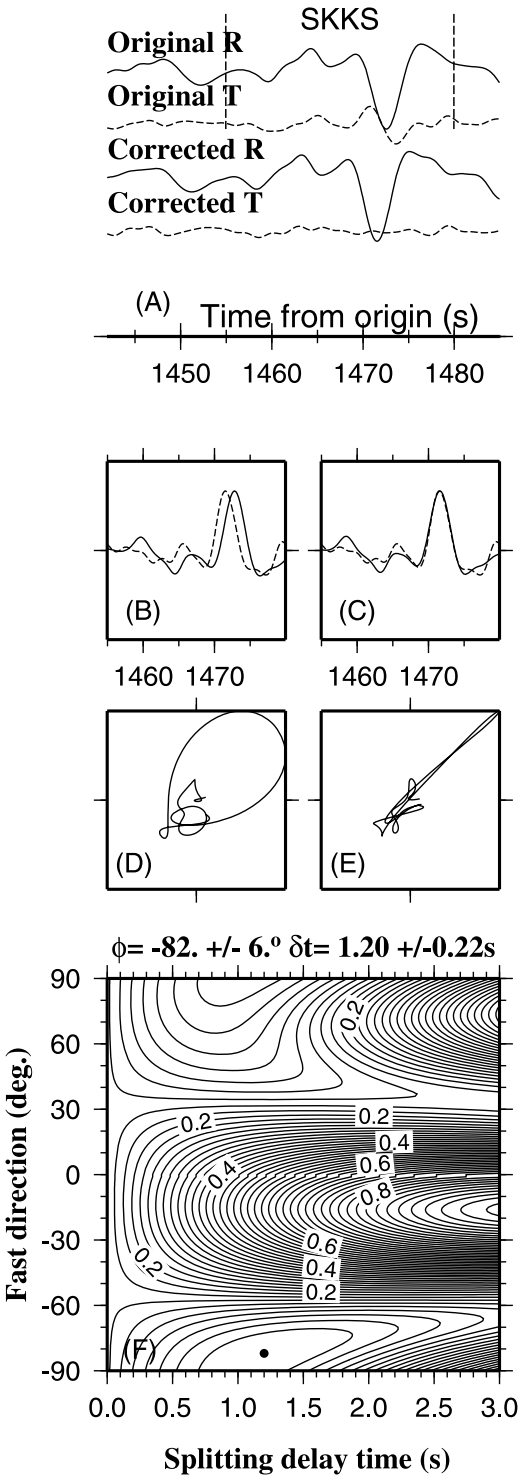

Figure 5. Same as Figure 4 but for an *SKKS* event from the NE.

continent, suggesting a single layer of anisotropy. A notable exception to this generalization is the study of *Barruol and Ben Ismail* [2001], who, based on 33 events recorded over the period of 1993–2000, recognized a difference in the splitting parameters between events among two azimuthal groups. However, because of the limited azimuthal coverage of the data set when the study was conducted, the $\pi/2$ periodicity was not recognized and the azimuth difference was attributed to "lateral heterogeneities in the upper mantle beneath this station" [*Barruol and Ben Ismail*, 2001]. The addition of 8 more years of data (2001–2008) led to the recognition of the clear $\pi/2$ periodicity shown in Figure 9,

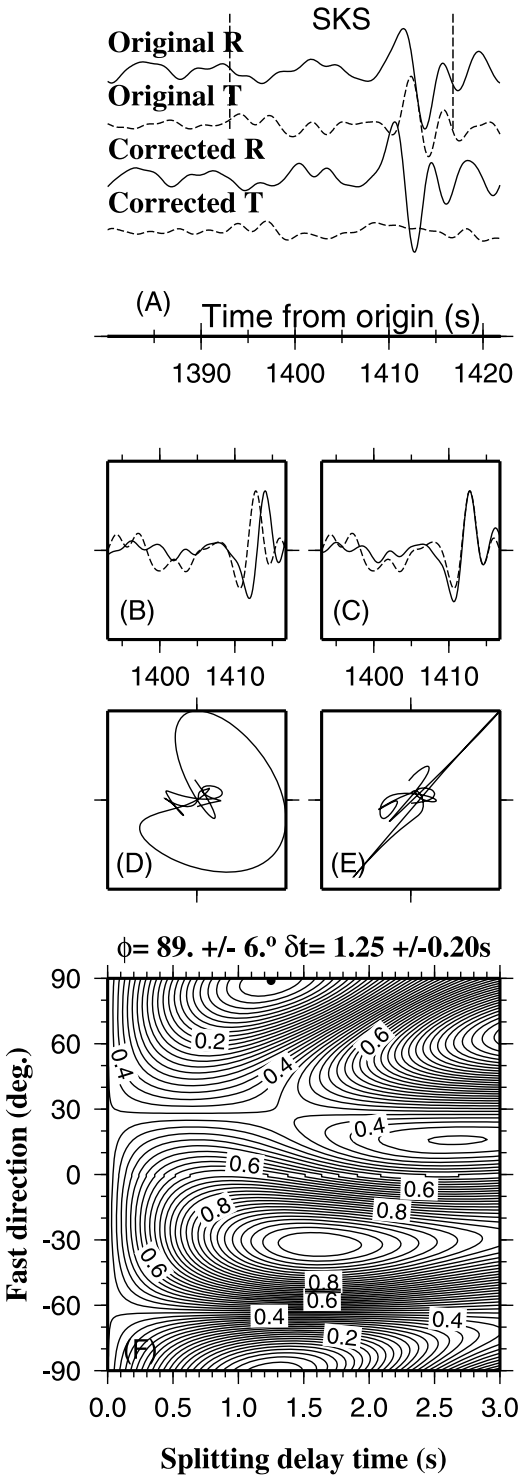

Figure 6. Same as Figure 4 but for station TEND and an event from the SW. Note the significant difference in the splitting parameters between this event and the one shown in Figure 4.

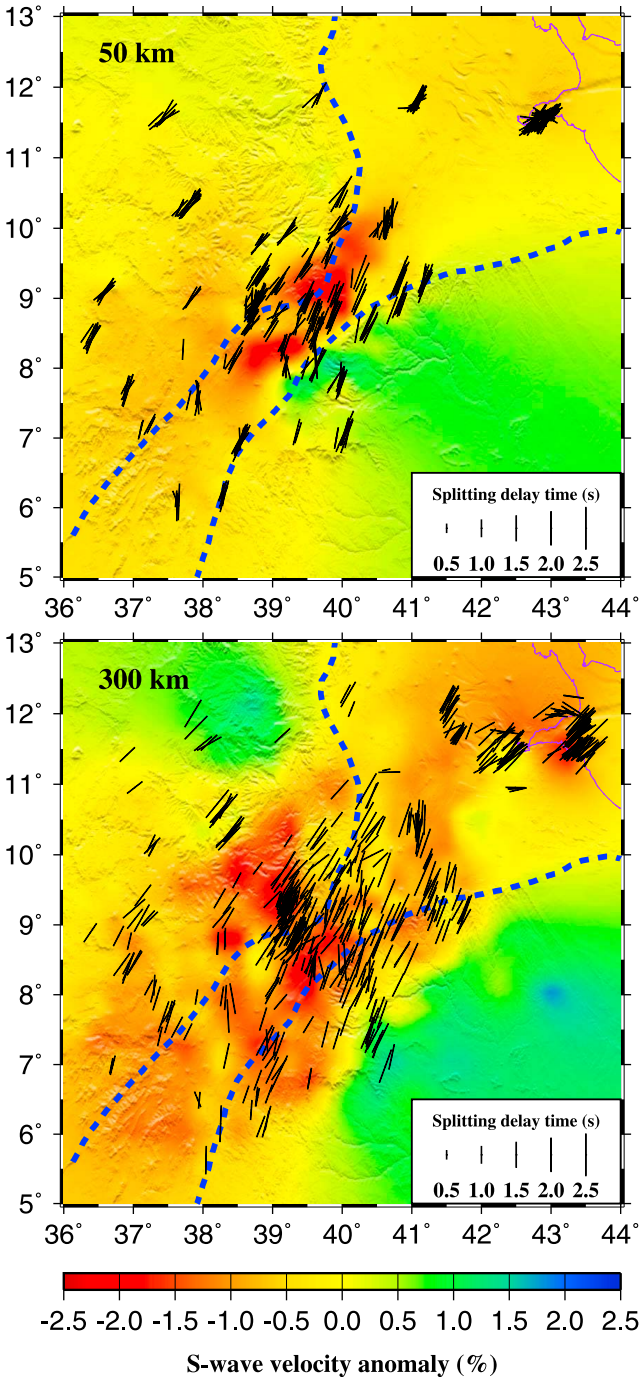

Figure 7. *XKS* splitting parameters plotted above ray-piercing points at depths of (top) 50 km and (bottom) 300 km. The color image in the background shows shear wave velocity anomalies at the corresponding depth based on the results of *Bastow et al.* [2008]. The dashed lines represent the boundaries of the MER and the Afar Depression.

vividly demonstrating the importance of long-running stations in recognizing complex anisotropy.

[14] Given the obvious $\pi/2$ periodicity, we grid search the four optimal splitting parameters under a two horizontal layer model [*Silver and Savage*, 1994] (see *Gao and Liu* [2009, equation (1)] for normalization and weighting parameters). Because the apparent splitting parameters are dependent on the dominant frequency of the *XKS* waveform [*Silver and Savage*, 1994], instead of using a uniform frequency as most previous studies did, we determine the peak frequency for each of the *XKS* waveforms and use it in the computation of the predicted apparent splitting parameters [*Gao and Liu*, 2009]. The resulting best fit model from the grid search has a fast direction of 38° and a splitting delay time of 2.0 s for the lower layer, and a fast direction of –71° and a delay time of 0.65 s for the upper layer (Figure 9), corresponding to a thickness of ~220 km and ~70 km for the lower and upper layer, respectively, for 4% anisotropy, or ~300 km and ~100 km for 3% anisotropy.

[15] It is well known that there are serious trade-offs between the four resulting splitting parameters from the grid search; that is, different sets of parameters can lead to similar goodness of fit between the observed and predicted values. To qualitatively estimate the uniqueness of the splitting parameters, *Gao and Liu* [2009] proposed a procedure to measure the scatteredness of the resulting parameters as a function of misfit between the observed and predicted splitting parameters. For each four-parameter set, a scaled misfit is calculated using $\lambda = 100(\chi^2 - \chi^2_{\min})/\chi^2_{\min}$ where χ^2 is the misfit corresponding to the 4 parameters, and $\chi^2_{\min}$ is the minimum misfit corresponding to the optimal set of parameters. The resulting scatteredness plots (Figure 10) suggest that the optimal two-layer parameters are fairly uniquely defined, especially the fast directions of both layers and the delay time of the upper layer.

[16] The fast direction for the top layer is subparallel to surface geological features including NW-SE trending propagators and associated normal faults in eastern Afar, as well as the orientation of crustal strain field revealed by focal mechanism solutions (Figure 2). The two-layer model is consistent with results from a surface wave anisotropy study, which suggests an approximately E-W fast direction in the top 175 km and a NE fast direction in the deeper layers in Afar [*Debayle et al.*, 2005]. A more recent surface wave tomography study [*Sicilia et al.*, 2008] also suggests a WNW trending fast direction in the top ~200 km and a mostly NE fast direction in the deeper layers. Note that a two-layer anisotropy may also exist beneath the Ethiopian Plateau and the MER, with the top layer being caused by MER-parallel magmatic dikes in the lithosphere, and the lower layer being associated with MER-parallel flow in the asthenosphere (see below). However, because the two layers have the same or similar fast directions, no azimuthal variations could be observed in this area (Figure 8).

3.2. Spatial Distribution of Anisotropy

[17] The way that the splitting parameters are displayed in Figure 7 does not provide insights into small spatial variations in the parameters. To amplify the variations, we first calculate the geographic location of the ray-piercing points at 300 km depth based on the IASP91 earth model, and then compute the average splitting parameters in overlapping rectangle blocks. The depth of 300 km is selected because when the source of anisotropy is placed at this depth, the measurements show the greatest spatial coherency (see section 4.1 below). The size of the blocks is 0.5° by 0.5° and the amount of overlap is 0.25°. A systematic spatial variation pattern is observed for both the fast directions and splitting

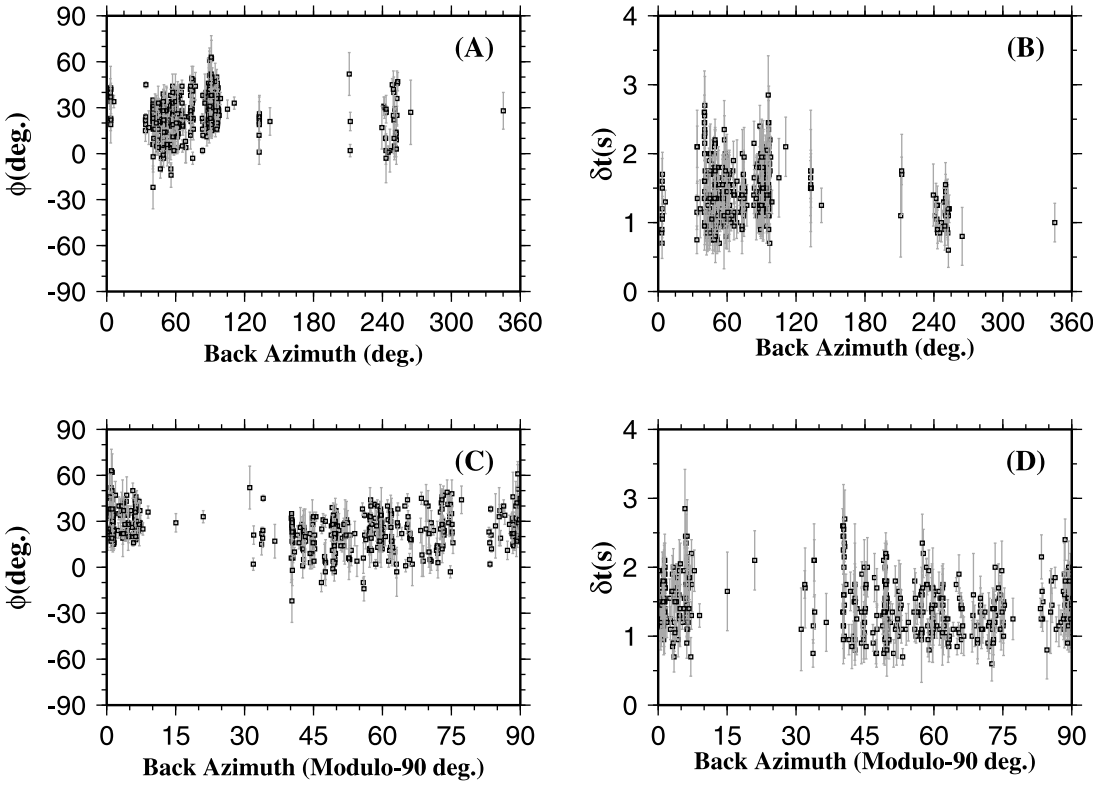

Figure 8. Azimuthal variations of resulting splitting parameters for stations on the Ethiopian Plateau and in the MER. (a) Fast directions plotted against the back azimuth. (b) Same as Figure 8a but for splitting delay times. (c) Fast directions plotted against modulo-90° of the back azimuth. (d) Same as Figure 8c but for splitting delay times. The modulo-90° plots are used to identify possible $\pi/2$ periodicity which is expected for two-layer anisotropy. For an event with a back azimuth α in the nth Cartesian quadrant (counted clockwise starting from the upper right quadrant), the corresponding modulo-90° of α is calculated using $\alpha_{90} = \alpha - (n - 1) \times 90°$.

delay times (Figure 11). On the NW side of the MER, the fast directions on the Ethiopian Plateau are mostly NE directed, while those on the SE side are more northerly directed (i.e., rotated counterclockwise relative to the former area). The mean fast directions between the two areas differ by about 20° (Figure 11). *Kendall et al.* [2005] identified this counterclockwise rotation using station-averaged fast directions in the close vicinity of the MER, and attributed it to magmatic segments which have a more northerly strike than the general strike of the MER. However, when data from stations in a broader area were used and when the results were plotted at their ray-piercing points (Figure 11), the area with more northerly fast directions extends at least 300 km to the south of the magmatic segments, suggesting that the rotation may not be related to the segments.

[18] Similar to previous studies [*Kendall et al.*, 2005, 2006], our results show that the area with the largest splitting delay time is located near the conjunction of the MER and the Afar Depression (Figure 11). However, our measurements do not support the conclusion that the MER axis corresponds to a zone of small delay times, and that more magmatic regions (Figure 11) have larger delay times [*Kendall et al.*, 2005, 2006]. The inconsistency in the conclusions is mostly due to the difference in data selection criteria, methods of data presentation (i.e., station-averaged versus individual measurements grouped by ray-piercing points), and the fact that stations away from the MER were not used by *Kendall et al.* [2005, 2006].

4. Discussion

4.1. Estimating the Depth of Anisotropy Beneath the MER and the Ethiopian Plateau

[19] Due to the steep incidence of the *XKS* raypaths, *XKS* splitting observations have excellent lateral resolution but low vertical resolution. Theoretically, the source of anisotropy can be at any depth from the core-mantle boundary to the surface. Because of the finite frequencies of the *XKS* waveform, the ray can be treated as a tube [*Alsina and Snieder*, 1996] approximately centered at the geometric raypath. The diameter of the tube increases with the dominant period and depth. The splitting parameters reflect the combined effect of seismic anisotropy inside the tube. A number of techniques were employed to estimate the width of the tube, including a Kirchoff integral approach [*Gao*, 1995; *Alsina and Snieder*, 1996], finite difference waveform forward modeling [*Rumpker and Ryberg*, 2000], and wave-equation Born approximation technique [*Favier and Chevrot*, 2003; *Long et al.* 2007]. An example raypath and its approximate sensitivity kernel are shown in Figure 12.

[20] Because most *XKS* waves have a nonvertical angle of incidence, for a layer of anisotropy at a given depth, the area

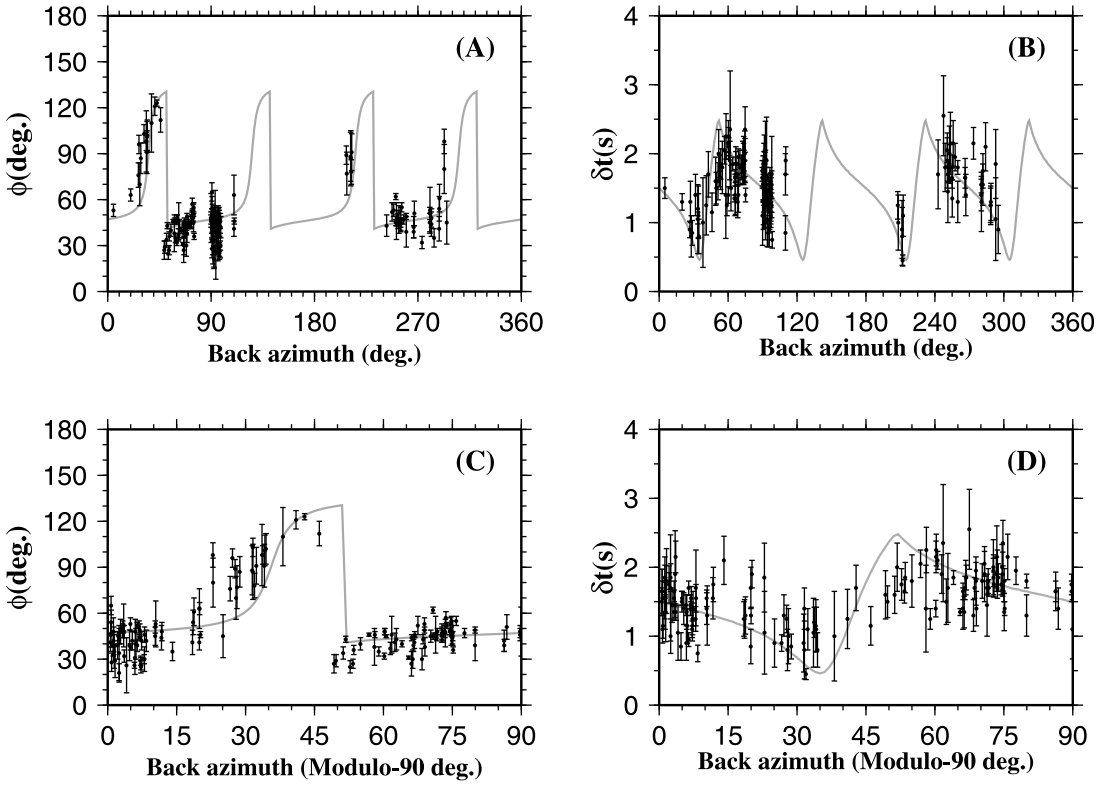

Figure 9. Same as Figure 8 but for data from the two stations (ATD and TEND) in the Afar Depression. The solid lines are theoretical results computed using a uniform frequency of 0.2 Hz and the optimal splitting parameters of the resulting two-layer model ($\phi = 38°$ and $\delta t = 2.0$ s for the lower layer, and $\phi = -71°$ and $\delta t = 0.65$ s for the upper layer).

sampled by the tube varies as a function of the back azimuth, epicentral distance, and focal depth of the event, as illustrated by the simple model shown in Figure 13. The seismic network in the model consists of 49 stations with 1° spacing in a 6° by 6° area centered at the Equator. The stations recorded two surface events, one from the north with an epicentral distance of 110° to the center of the network, and another from the south with the same epicentral distance. The center of a horizontal layer of anisotropy is placed at a depth of 300 km (Figure 12) with linearly varying splitting parameters defined by $\phi(r) = \phi_0 + c_1 \times r$, and $\delta t(r) = \delta t_0 + c_2 \times r$, where r is the distance (in degree) from the southwest corner of the network, $\phi_0 = 0°$, $\delta t_0 = 0.5$ s, $c_1 = 10°$/degree, and $c_2 = 0.2$ s/degree. Because the splitting parameters vary linearly, their mean values over a sensitivity kernel are approximately the same as the values at the actual ray-piercing points (Figure 12).

[21] When the measurements are placed above the ray-piercing points at the true depth of anisotropy (300 km), a high spatial coherency is observed in the splitting parameters between those from the two events because the two events sample the same areas in the overlapping zone (Figure 13a). On the other hand, when the measurements are placed above an incorrect depth, the spatial coherency reduces (Figure 13b). Obviously, a smaller difference between the assumed and the real depths leads to a smaller distance between the computed and true ray-piercing points, and consequently, results in a greater spatial coherency. Therefore, spatial coherency of observed splitting parameters can be used to estimate the depth of anisotropy beneath an area dominated by simple anisotropy (i.e., a single layer with horizontal axis of symmetry).

[22] We propose a procedure to estimate the depth of the center of the layer of anisotropy beneath the Ethiopian Plateau and the MER, where simple anisotropy is prevalent, by measuring the spatial coherency of the splitting parameters. The procedure includes the following steps:

[23] 1. Computing the geographic distribution of the ray-piercing points at a series of depths ranging from 0 to 600 km based on the IASP91 earth model, with a vertical interval of 5 km. Figure 7 shows the distribution of ray-piercing points at 50 and 300 km.

[24] 2. For each depth, calculating the sample standard deviation (STD) of the observed splitting parameters in 0.5° by 0.5° overlapping blocks. The distance between the center of neighboring blocks is 0.1°. A block is not used if the number of measurements in it is less than 4.

[25] 3. Calculating the variation factor F_v, for a given depth by averaging the STDs over all the blocks:

$$F_v = \frac{1}{N}\sum_{i=1}^{N}\sqrt{\frac{1}{M_i - 1}}\left(w_\phi\sqrt{\sum_{j=1}^{M_i}\left(\phi_{ij} - \overline{\phi_i}\right)^2} + w_{\delta t}\sqrt{\sum_{j=1}^{M_i}\left(\delta t_{ij} - \overline{\delta t_i}\right)^2}\right) \quad (1)$$

where N is the number of blocks, M_i is the number of measurements for the ith block, ϕ_{ij} and δt_{ij} are the jth fast direction and splitting delay time measurement in the ith block, $\overline{\phi_i}$ and $\overline{\delta t_i}$ are the averages over all the measurements

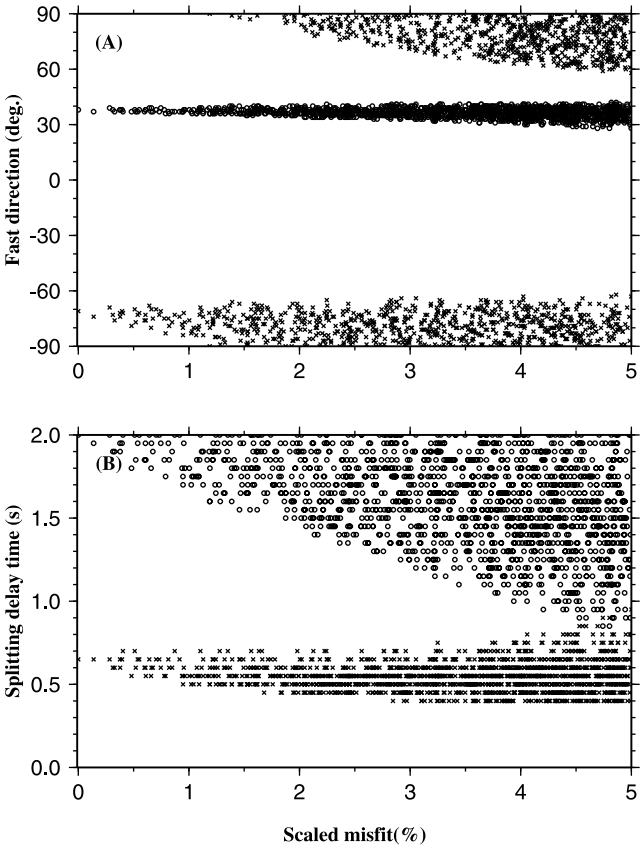

Figure 10. Possible two-layer splitting parameters plotted against scaled misfit. (a) Fast directions; (b) splitting delay times. For both plots, the splitting parameters for the lower layer are plotted as circles, and those for the upper layer are plotted as crosses.

in block i, and w_ϕ and $w_{\delta t}$ are the weighting factor for the ϕ and δt measurements, respectively. Because the ϕ measurements have a maximum of 180° and the δt measurements have a maximum of about 2.5 s, we use $w_\phi = 1/180°$ and $w_{\delta t} = 0.4$ s so that the misfits of the two parameters can be combined.

[26] The resulting F_v, which is a dimensionless factor reflecting the spatial variation of the measurements as a function of assumed depth of anisotropy, shows a clear minimum at the depth of about 300 km (Figure 14), suggesting that the main source of anisotropy is centered at about 300 km and thus is in the asthenosphere. This conclusion is consistent with result of recent surface wave tomography studies [*Debayle et al.*, 2005; *Sicilia et al.*, 2008] which detected a persistent NE directed anisotropy in the asthenosphere beneath the MER and the Afar Depression.

[27] The success of using the above procedure to estimate the depth of observed anisotropy is dependent on a number of factors. First, there must be spatial variations in the splitting parameters. Second, the source of anisotropy must be in a single layer with horizontal axis of symmetry. Complex anisotropy such as multiple layers and/or dipping axes leads to azimuthal (and piercing point location) dependence in the observed splitting parameters, and thus will increase the STDs. Third, the stations must be close enough relative to the depth of the anisotropic layer, so that the sensitivity kernels at the depth of the anisotropic layer from different raypaths partially or entirely overlap. Fourth, a decent azimuthal coverage is required, although it is unnecessary for the raypaths to have opposite back azimuths or the same ray parameters. For the study area, the above conditions are all satisfied, except for stations ATD and TEND which show azimuthal variations in the splitting parameters (thus do not satisfy the second criterion above) and were excluded from the computation of F_v. Consequently, the optimal depth of anisotropy beneath the Afar Depression remains unconstrained. Given the close proximity, similarities in tectonic history and present tectonic environment, and similar seismic tomography

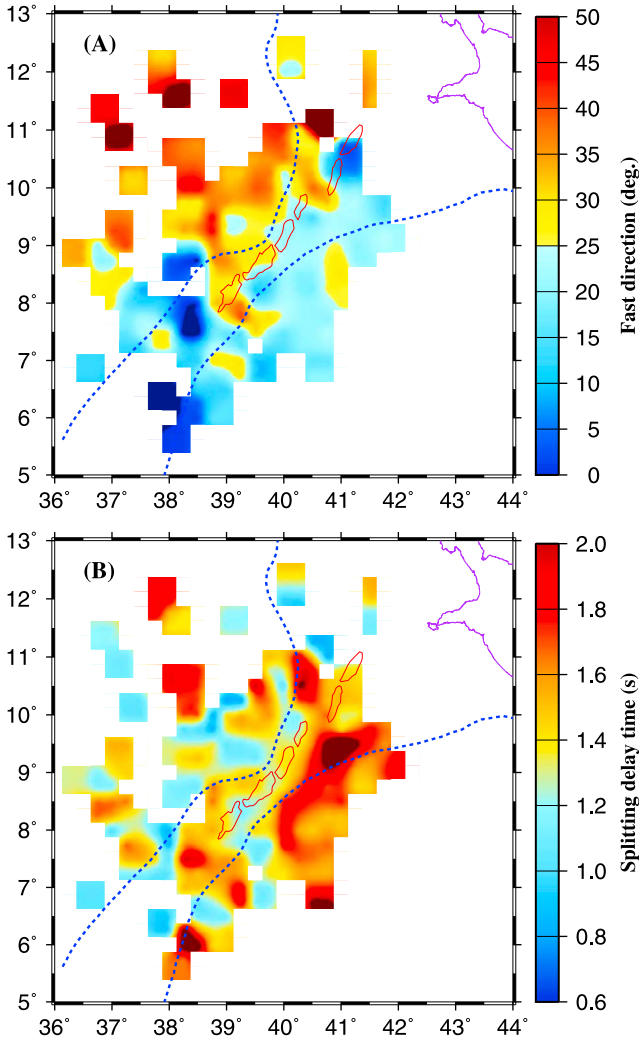

Figure 11. Spatial distribution of (a) fast directions and (b) splitting delay times for the Ethiopian Plateau and the MER. To obtain the plots, splitting parameters with ray-piercing points (at 300 km depth) in the same 0.5° × 0.5° blocks are averaged (see section 3.2 in the text) and the resulting distribution of the averages are fitted using a continuous surface gridding algorithm with a tension factor of 0.5 [*Smith and Wessel*, 1990]. Blocks without measurements are not plotted. Also plotted are the magmatic segments (areas outlined by solid red lines) and the boundaries of the MER and the Afar Depression (dashed lines).

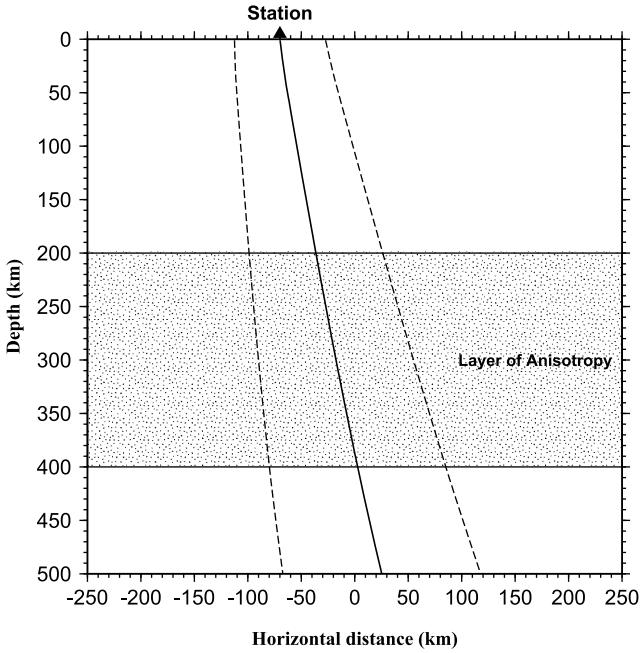

Figure 12. Schematic diagram showing an *SKS* raypath of a surface event with a distance of 110° from a recording station calculated using the IASP91 earth model. The two bordering dashed lines represent the boundaries of the sensitivity kernel for a shear wave with a period of 8 s based on the results of *Favier and Chevrot* [2003]. The shaded area represents a layer of anisotropy with arbitrary thickness centered at 300 km deep.

structures in the asthenosphere (Figure 7b) between the MER and Afar, in following discussions we assume that the depth of anisotropy in the asthenosphere is similar beneath the two areas (note that the asthenosphere is the bottom layer beneath Afar). It must be mentioned that as long as the asthenosphere (and not the lithosphere) is the major contributor for the observed anisotropy in Afar (and this is probably true given the thickness of the two layers discussed in section 3.1), a more accurate estimate of the depth is insignificant in reaching the main conclusions of the study.

4.2. Possible Causes of Observed Seismic Anisotropy

[28] In the upper mantle, the causes of anisotropy detectable by *XKS* splitting can be grouped into two general categories. The first category is lattice preferred orientation (LPO) of anisotropic minerals such as olivine [*Nicolas and Christensen*, 1987], wadsleyite [*Tommasi et al.*, 2004], and serpentine [*Katayama et al.*, 2009] developed under strain fields such as shortening and shearing. The second category is shape-preferred orientation formed by preferably aligned vertical magmatic dikes.

[29] In continental areas dominated by extensional structures, possible processes causing seismic anisotropy include lithospheric shortening associated with past collisional events, vertical magmatic dikes associated with the development of the MER and Afar, and plastic flow in the asthenosphere [*Gao et al.*, 1994, 1997; *Vauchez et al.*, 2000]. In the following we analyze each of the possibilities and discuss their contributions to the observed anisotropy, on the basis of the potential lateral, depth, and azimuthal variations of anisotropy.

4.2.1. Precambrian Lithospheric Sutures

[30] Many of the world's present and past zones of continental collision are characterized by mountain belt–parallel fast directions, due to preferred alignment of olivine *a* axis in the direction perpendicular to shortening [e.g., *McNamara et al.*, 1994; *Li and Chen*, 2006; *Gao et al.*, 2008]. *Gashawbeza et al.* [2004] used this mechanism to propose that the observed seismic anisotropy under the entire Ethiopian Plateau is due to

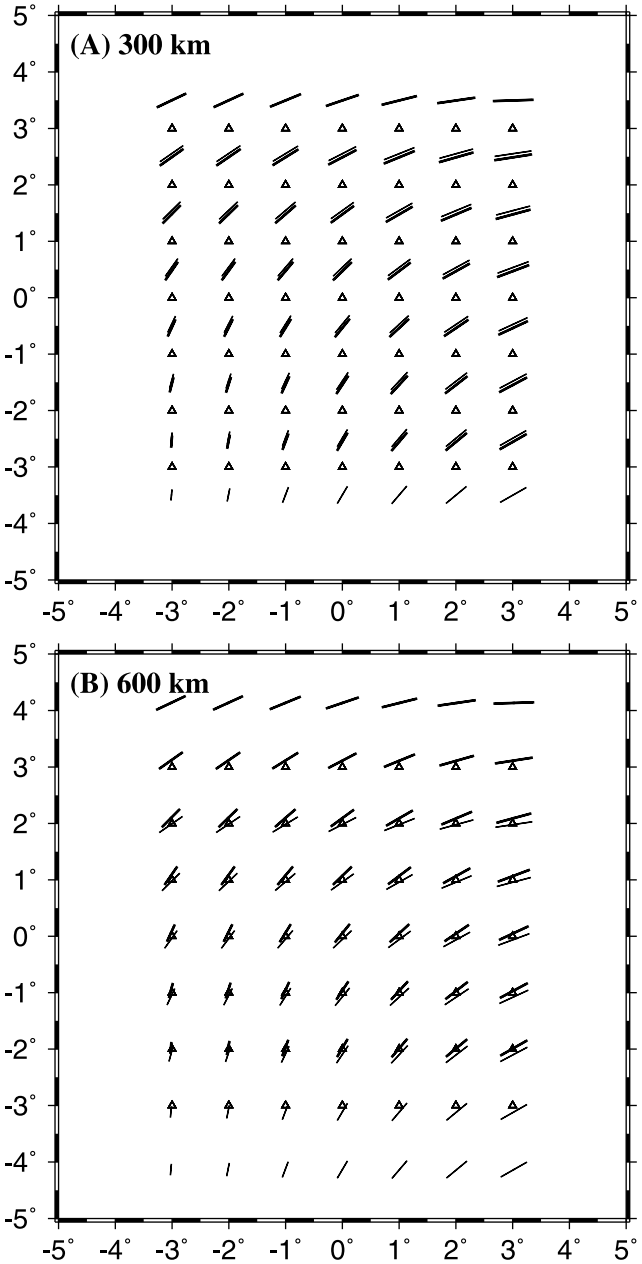

Figure 13. Spatial distribution of synthetic shear wave splitting parameters plotted above ray-piercing points at (a) 300 km depth, which is the actual depth of the center of the layer of anisotropy, and (b) 600 km depth. Thick (thin) bars represent splitting parameters from a surface event with an epicentral distance of 110° and a back azimuth of 0° (180°). Triangles represent seismic stations.

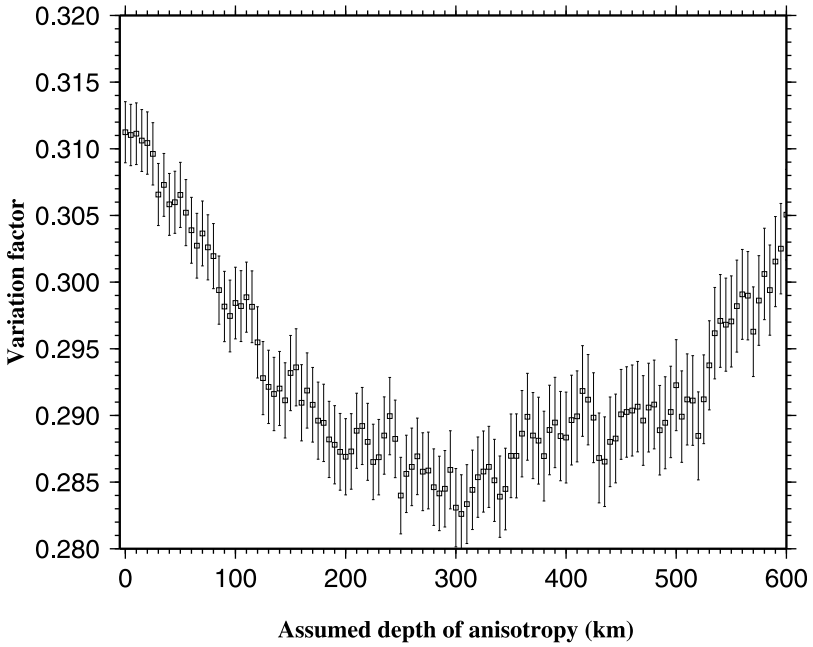

Figure 14. Spatial variation factor as a function of assumed depth of the source of anisotropy.

the presence of Neoproterozoic lithospheric sutures of the East African Orogen, which are subparallel to the MER in the vicinity of the rift and is approximately N-S in central and northern Ethiopia (Figure 2) [*Berhe*, 1990; *Abdelsalam and Stern*, 1996]. While this model can explain the observations in the MER, it is inconsistent with the large (about 30°) difference between the N-S trending sutures and the observed NE fast directions in NW Ethiopia. Additionally, this mechanism cannot explain the WNW oriented fast directions in the upper layer in Afar and the observed large splitting delay times because the Neoproterozoic lithosphere is expected to be thinned significantly beneath Afar [*Ayele et al.*, 2004; *Bastow et al.*, 2005]. Thus, if Precambrian lithospheric sutures are mostly responsible for the observed splitting, the anticipated splitting delay times in Afar should be smaller, not larger (as observed), than those observed on the Ethiopian Plateau.

4.2.2. Vertical Magmatic Dikes

[31] In areas of extended lithosphere such as continental rifts and passive continental margins, rift-parallel vertical magmatic dikes form a transverse isotropy with horizontal rift-orthogonal axis of symmetry. This mechanism has been used to explain rift-parallel fast directions [*Gao et al.*, 1997, 2008; *Kendall et al.*, 2005, 2006]. Based on the observation that the fast directions in the vicinity of the MER are mostly rift parallel, *Kendall et al.* [2005, 2006] proposed that aligned melt intrusion zones in the MER are the dominant mechanism for the observed seismic anisotropy.

[32] There are several lines of evidence arguing against magmatic dikes being the dominant cause of the observed anisotropy. First, as shown above, the depth of the dominant source of anisotropy is about 300 km, which is significantly deeper than the base of the lithosphere in the study area which is less than 100 km based on most of the previous geophysical studies [e.g., *Pasyanos*, 2010]. Second, there is a general lack of correspondence between the spatial distribution of the observed splitting parameters (Figure 7) and locations of lithospheric dikes revealed by active source seismic experiments [*Keranen et al.*, 2004; *Maguire et al.*, 2006] and surface observations (Figure 11). The expected larger splitting delay times above those locations are not observed. Third, the diking origin model cannot explain the two-layer structure observed in Afar. The dike origin model, if it is applicable to the NW-SE strike Red Sea and Gulf of Aden propagators in Afar, would predict azimuthally independent NW-SE fast directions in Afar. Such a simple pattern is not observed. Instead, a two-layer model is required by the data (Figure 9). If we assume that the upper layer of anisotropy is from magmatic dikes in the lithosphere, its small (0.65 s versus 2.0 s for the lower layer) delay time suggests that the dikes contribute only about 1/4 of the total delay time.

4.2.3. Asthenospheric Flow

[33] Our spatial coherency depth estimator suggests an optimal depth of 300 km beneath the MER and the Ethiopian Plateau, implying that LPO of olivine developed in the asthenosphere is the major contributor of the observed anisotropy. Previous studies [e.g., *Vinnik et al.*, 1989; *Marone and Romanowicz*, 2007; *Liu*, 2009] indicate that absolute plate motion (APM) can lead to LPO development with a fast direction parallel to APM. In the study area, however, the APM rate is small (about 1.7 cm/yr) and the direction is about 73° counterclockwise from the North [*Gripp and Gordon*, 2002] (Figure 1), which is almost exactly perpendicular to the majority of the fast directions. Therefore, APM of the African plate is not likely a major contributor of the observed anisotropy. This suggests that APM-related LPO, if it exists, is overprinted by a NE oriented flow system.

[34] The spatial and azimuthal distributions of the splitting parameters reported here and the resulting optimal depth of anisotropy can be best explained by a model involving NE directed flow in the asthenosphere beneath the study area. The existence of such a flow system, which is expected to

have a higher degree of partial melt and higher temperature than surrounding regions at the same depths, has been suggested previously by *XKS* splitting studies [e.g., *Barruol and Ben Ismail*, 2001; *Ayele et al.*, 2004] and is supported by seismic body and surface wave tomography and receiver function studies [*Grand*, 2002; *Ayele et al.*, 2004; *Bastow et al.*, 2005, 2008; *Dugda et al.*, 2005, 2007; *Keranen et al.*, 2004, 2009; *Benoit et al.*, 2006; *Pasyanos*, 2010], which, in spite of inconsistencies in the spatial distribution and magnitude of the anomalies, all suggest a broad low-velocity (and thus hot) zone in the uppermost 400 km beneath the study area (Figure 7). Given the dominantly N-S oriented *XKS* fast directions observed in Saudi Arabia [*Wolfe et al.*, 1999; *Hansen et al.*, 2006] (Figure 1), we speculate that the flow continues northward to northern Saudi Arabia after it passes the junction area between the Red Sea and the Gulf of Aden. Indeed, the presence of mantle flow under the Arabian plate was suggested by *Hansen et al.* [2006] based on shear wave splitting measurements in Saudi Arabia. Unfortunately, a lack of seismic stations on the African side of the Red Sea resulted in limited spatial resolution of mantle tomographic images and a complete paucity of *XKS* splitting measurements in Somalia, Eritrea, Sudan, and southern Egypt (Figure 1), and consequently, the lateral extent of the speculated mantle flow cannot be constrained. However, numerous observations including the sharp topographic and magmatic asymmetries across the Red Sea [*Daradich et al.*, 2003; *Bosworth et al.*, 2005] suggest that the northward mantle flow may only exist beneath the Arabian side, and is responsible for the opening of the Red Sea [*Abdelsalam and Gao*, 2009].

4.3. Implications on the Existence and Strength of the Afar Plume

[35] Although it was suggested that basal erosion by an actively rising mantle plume is needed to form the Afar Depression [*Hempton*, 1987; *Schilling et al.*, 1992], the existence, location, strength, geochemical and isotopic signatures, and the number of plume heads of the so-called Afar plume are still heavily debated topics [e.g., *Ebinger and Sleep*, 1998; *Furman*, 2007]. While an active plume is the most likely source of the NE directed flow suggested by the shear wave splitting measurements, the anticipated radial or parabolic patterns of fast directions observed at the Hawaii and Eifel hot spots [*Walker et al.*, 2005] are not observed in the study area. In addition, laboratory experiments suggest that in the vicinity of a plume center, a complicated pattern of splitting parameters is expected, and in the case of A-type olivine fabrics, small splitting delay times are anticipated [*Karato et al.*, 2008].

[36] The dominantly NE directed asthenospheric flow pattern inferred from the *XKS* splitting measurements, the large splitting delay times relative to global average suggest that an active mantle plume is unlikely to be located beneath the study area. This conclusion is similar to previous *XKS* splitting studies [e.g., *Gashawbeza et al.*, 2004]. Alternatively, if there is indeed a plume beneath Afar, as recently suggested by seismic tomography [*Montelli et al.*, 2004; *Sicilia et al.*, 2008] and geochemical studies [e.g., *Marty et al.*, 1996], the strength of the vertical component of the flow in the upper mantle must be relatively weaker than that of the horizontal flow, which might originate from another plume located beneath southern Kenya or northern Tanzania, as suggested by previous geophysical and geochemical studies [e.g., *Nyblade et al.*, 2000; *Courtillot et al.*, 2003].

5. Conclusions

[37] Shear wave splitting analysis using all available broadband seismic data recorded in the Afar Depression and adjacent areas reveal systematic spatial and azimuthal variations of the approximately 600 pairs splitting parameters. Using the spatial coherency of the splitting parameters observed in the MER and on the Ethiopian Plateau, the optimal depth of the source of anisotropy is placed at 300 km, suggesting that olivine LPO in the asthenosphere is the major cause of the observed MER-parallel seismic anisotropy. In the Afar Depression, a two-layer model of anisotropy is revealed by the systematic variations of the splitting parameters with a $\pi/2$ periodicity. The top layer has a small splitting delay time of 0.65 s and a WNW fast direction parallel to the local strike of the Red Sea and Gulf of Aden propagators and associated normal faults and magmatic dikes. The lower layer has a large splitting delay time of 2.0 s and an NE fast direction that is identical to the dominant fast directions observed on the Ethiopian Plateau and in the MER. The resulting two-layer model suggests that fabrics in the lithosphere contribute about 1/4 of the observed anisotropy, and the rest is from NE directed flow in the asthenosphere.

[38] Results from this study, when combined with results from seismic body and surface wave tomography, shear wave splitting measurements in surrounding areas, and surface geological observations, support a model in which NE directed flow in the asthenosphere is the dominant source of the observed anisotropy. The flow might originate from an active mantle plume in southern Kenya or northern Tanzania, and continues northward beneath Saudi Arabia. This conclusion is inconsistent with previous XKS splitting studies which attributed the observed anisotropy to magmatic dikes [*Kendall et al.*, 2005, 2006] or Precambrian sutures [*Gashawbeza et al.*, 2004].

[39] Finally, as demonstrated in this study and elsewhere (e.g., *Gao and Liu* [2009] for southern Tibet), long-running seismic stations are essential in the recognition of complex seismic anisotropy and consequently in revealing geodynamic processes in the Earth's interior.

[40] **Acknowledgments.** We thank the participants of the EAGLE and EBSE projects and the IRIS DMC for providing the high-quality seismic data used in the study and Ian Bastow for providing seismic tomographic results [*Bastow et al.*, 2008]. A. Elsheikh helped with digitizing the tectonic boundaries shown in Figure 2. Constructive reviews from two reviewers and the Associate Editor significantly improved the paper. The work is supported by NSF awards EAR-0739015 and EAR-0911346 and by Statoil A.S.A. This article is Missouri University of Science and Technology Geology and Geophysics contribution 22.

References

Abdelsalam, M. G., and S. S. Gao (2009), Origin of initial rifting in the Red Sea: Was it vertical tectonics?, *Geol. Soc. Am. Abstr. Programs*, *41*(7), 127.

Abdelsalam, M. G., and R. J. Stern (1996), Sutures and shear zones in the Arabian-Nubian shield, *J. Afr. Earth Sci.*, *23*, 289–310.

Acocella, V., B. Abebe, T. Korme, and F. Barberi (2008), Structure of Tendaho Graben and Manda Hararo Rift: Implications for the evolution of the southern Red Sea propagator in Central Afar, *Tectonics*, *27*, TC4016, doi:10.1029/2007TC002236.

Alsina, D., and R. Snieder (1996), Constraints on the velocity structure beneath the Tornquist-Teisseyre zone from beamforming analysis, *Geophys. J. Int.*, *126*, 205–218.

Ayele, A., G. Stuart, and J.-M. Kendall (2004), Insights into rifting from shear wave splitting and receiver functions: An example from Ethiopia, *Geophys. J. Int.*, *157*, 354–362.

Ayele, A., E. Jacques, M. Kassim, T. Kidane, A. Omar, S. Tait, A. Nercessian, J.-B. de Chabalier, and G. King (2007), The volcano-seismic crisis in Afar, Ethiopia, starting September 2005, *Earth Planet. Sci. Lett.*, *255*, 177–187.

Barruol, G., and W. Ben Ismail (2001), Upper mantle anisotropy beneath African IRIS and Geoscope stations, *Geophys. J. Int.*, *146*, 549–561.

Barruol, G., and R. Hoffmann (1999), Upper mantle anisotropy beneath the Geoscope stations, *J. Geophys. Res.*, *104*, 10,757–10,773.

Bastow, I. D., G. W. Stuart, J.-M. Kendall, and C. J. Ebinger (2005), Upper-mantle seismic structure in a region of incipient continental breakup: northern Ethiopian rift, *Geophys. J. Int.*, *162*, 479–493.

Bastow, I. D., A. A. Nyblade, G. W. Stuart, T. Rooney, and M. H. Benoit (2008), Upper mantle seismic structure beneath the Ethiopian hotspot: Rifting at the edge of the African low velocity anomaly, *Geochem. Geophys. Geosyst.*, *9*, Q12022, doi:10.1029/2008GC002107.

Ben Ismail, W., and D. Mainprice (1998), An olivine fabric database: An overview of upper mantle fabrics and seismic anisotropy, *Tectonophysics*, *296*, 145–158.

Benoit, M. H., A. A. Nyblade, and J. C. VanDecar (2006), Upper mantle *P*-wave speed variations beneath Ethiopia and the origin of the Afar hotspot, *Geology*, *34*, 329–332.

Berhe, S. M. (1990), Ophiolites in northeast and East Africa: Implications for Proterozoic crustal growth, *J. Geol. Soc. London*, *147*, 41–57.

Beyene, A. M., and M. G. Abdelsalam (2005), Tectonics of the Afar depression: A review and synthesis, *J. Afr. Earth Sci.*, *41*, 41–59.

Birch, F. (1960), The velocity of compressional waves in rocks to 10 kilobars, Part 1, *J. Geophys. Res.*, *65*, 1083–1102.

Bosworth, W., P. Huchon, and K. McClay (2005), The Red Sea and Gulf of Aden Basins, *J. Afr. Earth Sci.*, *43*, 334–378.

Coffin, M. F., and O. Eldholm (1994), Large igneous provinces: crustal structure, dimensions, and external consequences, *Rev. Geophys.*, *32*, 1–36.

Courtillot, V., A. Davaille, J. Besse, and J. Stock (2003), Three distinct types of hotspots in the Earth's mantle, *Earth Planet. Sci. Lett.*, *205*, 295–308.

Daradich, A., J. X. Mitrovica, R. N. Pysklywec, S. D. Willett, and A. M. Forte (2003), Mantle flow, dynamic topography, and rift-flank uplift of Arabia, *Geology*, *31*, 901–904.

Debayle, E., B. Kennett, and K. Priestley (2005), Global azimuthal seismic anisotropy and the unique plate-motion deformation of Australia, *Nature*, *433*, 509–512, doi:10.1038/nature03247.

Dugda, M. T., A. A. Nyblade, J. Julia, C. A. Langston, C. J. Ammon, and S. Simiyu (2005), Crustal structure in Ethiopia and Kenya from receiver function analysis: Implications for rift development in eastern Africa, *J. Geophys. Res.*, *110*, B01303, doi:10.1029/2004JB003065.

Dugda, M. T., A. A. Nyblade, and J. Julia (2007), Thin lithosphere beneath the Ethiopian Plateau revealed by a joint inversion of Rayleigh wave group velocities and receiver functions, *J. Geophys. Res.*, *112*, B08305, doi:10.1029/2006JB004918.

Ebinger, C. J., and M. Casey (2001), Continental breakup in magmatic provinces: An Ethiopian example, *Geology*, *29*, 527–530.

Ebinger, C. J., and N. Sleep (1998), Cenozoic magmatism throughout east Africa resulting from impact of one large plume, *Nature*, *395*, 788–791.

Favier, N., and S. Chevrot (2003), Sensitivity kernels for shear wave splitting in transverse isotropic media, *Geophys. J. Int.*, *153*, 213–228.

Fouch, M. J., and S. Rondenay (2006), Seismic anisotropy beneath stable continental interiors, *Phys. Earth Planet. Inter.*, *158*, 292–320, doi:10.1016/j.pepi.2006.03.024.

Furman, T. (2007), Geochemistry of East African Rift basalts: An overview, *J. Afr. Earth Sci.*, *48*, 147–160.

Gao, S. (1995), Seismic evidence for small-scale mantle convection under the Baikal rift zone, Siberia, Ph.D. dissertation, 221 pp., Univ. of Calif., Los Angeles.

Gao, S. S., and K. H. Liu (2009), Significant seismic anisotropy beneath the southern Lhasa Terrane, Tibetan Plateau, *Geochem. Geophys. Geosyst.*, *10*, Q02008, doi:10.1029/2008GC002227.

Gao, S., P. M. Davis, H. Liu, P. D. Slack, Y. A. Zorin, V. V. Mordvinova, V. M. Kozhevnikov, and R. P. Meyer (1994), Seismic anisotropy and mantle flow beneath the Baikal rift zone, *Nature*, *371*, 149–151.

Gao, S. S., P. M. Davis, K. H. Liu, P. D. Slack, A. W. Rigor, Y. A. Zorin, V. V. Mordvinova, V. M. Kozhevnikov, and N. A. Logatchev (1997), *SKS* splitting beneath continental rift zones, *J. Geophys. Res.*, *102*, 22,781–22,797.

Gao, S. S., K. H. Liu, R. J. Stern, G. R. Keller, J. P. Hogan, J. Pulliam, and E. Y. Anthony (2008), Characteristics of mantle fabrics beneath the south-central United States: Constraints from shear-wave splitting measurements, *Geosphere*, *4*, 411–417, doi:10.1130/GES00159.1.

Gashawbeza, E. M., S. L. Klemperer, A. A. Nyblade, K. T. Walker, and K. M. Keranen (2004), Shear-wave splitting in Ethiopia; Precambrian mantle anisotropy locally modified by Neogene rifting, *Geophys. Res. Lett.*, *31*, L18602, doi:10.1029/2004GL020471.

Grand, S. P. (2002), Mantle shear-wave tomography and the fate of subducted slabs, *Philos. Trans. R. Soc.*, *360*, 2475–2491.

Gripp, A. E., and R. G. Gordon (2002), Young tracks of hotspots and current plate velocities, *Geophys. J. Int.*, *150*, 321–364.

Hansen, S., S. Schwartz, A. Al-Amri, and A. Rodgers (2006), Combined plate motion and density-driven flow in the asthenosphere beneath Saudi Arabia: Evidence from shear-wave splitting and seismic anisotropy, *Geology*, *34*, 869–872, doi:10.1130/G22713.1.

Hempton, M. R. (1987), Constraints on Arabian plate motion and extension history of the Red Sea, *Tectonics*, *6*, 687–705.

Hoffmann, C., V. Courtillot, G. Feraud, P. Rochette, G. Yirgu, E. Ketefo, and R. Pik (1997), Timing of the Ethiopian flood basalt event and implications for plume birth and global change, *Nature*, *389*, 838–841.

Karato, S., H. Jung, I. Katayama, and P. Skemer (2008), Geodynamic significance of seismic anisotropy of the upper mantle: New insights from laboratory studies, *Annu. Rev. Earth Planet. Sci.*, *36*, 59–95.

Katayama, I., K.-I. Hirauchi, K. Michibayashi, and J.-I. Ando (2009), Trench-parallel anisotropy produced by serpentine deformation in the hydrated mantle wedge, *Nature*, *461*, 1114–1117.

Kendall, J.-M., G. W. Stuart, C. Ebinger, I. D. Bastow, and D. Keir (2005), Magma-assisted rifting in Ethiopia, *Nature*, *433*, 146–148.

Kendall, J.-M., S. Pilidou, D. Keir, I. D. Bastow, G. W. Stuart, and A. Ayele (2006), Mantle upwellings, melt migration and rifting of Africa: Insights from seismic anisotropy, in *The Afar Volcanic Province Within the East African Rift System*, edited by G. Yirgu et al., *Geol. Soc. Spec. Publ.*, 259, 55–72.

Keranen, K., S. L. Klemperer, R. Gloaguen, and EAGEL working group (2004), Three-dimensional seismic imaging of a protoridge axis in the Main Ethiopian rift, *Geology*, *32*, 949–952, doi:10.1130/G20737.1.

Keranen, K., S. L. Klemperer, J. Julia, J. L. Lawrence, and A. Nyblade (2009), Low lower-crustal velocity across Ethiopia: Is the Main Ethiopian Rift a narrow rift in a hot craton?, *Geochem. Geophys. Geosyst.*, *10*, Q0AB01, doi:10.1029/2008GC002293.

Li, A., and C. Chen (2006), Shear-wave splitting beneath the central Tien Shan and tectonic implications, *Geophys. Res. Lett.*, *33*, L22303, doi:10.1029/2006GL027717.

Liu, K. H. (2009), NA-SWS-1.1: A uniform database of teleseismic shear-wave splitting measurements for North America, *Geochem. Geophys. Geosyst.*, *10*, Q05011, doi:10.1029/2009GC002440.

Liu, K. H., S. S. Gao, Y. Gao, and J. Wu (2008), Shear-wave splitting and mantle flow associated with the deflected Pacific slab beneath northeast Asia, *J. Geophys. Res.*, *113*, B01305, doi:10.1029/2007JB005178.

Long, M. D., and P. G. Silver (2009), Shear wave splitting and mantle anisotropy: Measurements, interpretations, and new directions, *Surv. Geophys.*, *30*, 407–461.

Long, M. D., B. H. Hager, M. V. de Hoop, and R. D. van der Hilst (2007), Two-dimensional modeling of subduction zone anisotropy and application to southwestern Japan, *Geophys. J. Int.*, *170*, 839–856, doi:10.1111/j.1365-246X.2007.03464.x.

Maguire, P. K. H., et al. (2003), Geophysical project in Ethiopia studies continental breakup, *Eos Trans. AGU*, *84*, 337–340.

Maguire, P., G. R. Keller, S. Klemperer, G. Mackenzie, S. Harder, B. O'Reilly, H. Thybo, L. Asfaw, M. Khan, and M. Amha (2006), Crustal structure of the northern Main Ethiopian Rift from the EAGLE controlled source survey: A snapshot of incipient lithospheric breakup, in *The Afar Volcanic Province Within the East African Rift System*, edited by G. Yirgu et al., *Geol. Soc. Spec. Publ.*, 259, 269–291.

Marone, F., and B. Romanowicz (2007), The depth distribution of azimuthal anisotropy in the continental upper mantle, *Nature*, *447*, 198–201.

Marty, B., R. Pik, and G. Yirgu (1996), Helium isotopic variations in Ethiopian plume lavas: Nature of magmatic sources and limit on lower mantle contribution, *Earth Planet. Sci. Lett.*, *144*, 223–237.

McNamara, D. E., T. J. Owens, P. G. Silver, and F. T. Wu (1994), Shear wave anisotropy beneath the Tibetan Plateau, *J. Geophys. Res.*, *99*, 13,655–13,665.

Montelli, R., G. Nolet, F. A. Dahlen, G. Masters, E. R. Engdahl, and S.-H. Hung (2004), Finite-frequency tomography reveals a variety of plumes in the mantle, *Science*, *303*, 338–343.

Nicolas, A., and N. I. Christensen (1987), Formation of anisotropy in upper mantle peridotites: A review, in *Composition, Structure, and Dynamics*

of the Lithosphere-Asthenosphere System, *Geodyn. Ser.*, vol. 16, edited by K. Fuchs and C. Froidevaux, pp. 111–123, AGU, Washington, D. C.
Nyblade, A. A., and C. A. Langston (2002), Broadband seismic experiments probe the East African rift, *Eos Trans. AGU*, *83*(37), 405–408.
Nyblade, A. A., T. J. Owens, H. Gurrola, J. Ritsema, and C. A. Langston (2000), Seismic evidence for a deep upper mantle thermal anomaly beneath east Africa, *Geology*, *28*, 599–602.
Pasyanos, M. E. (2010), Lithospheric thickness modeled from long-period surface wave dispersion, *Tectonophysics*, *481*, 38–50, doi:10.1016/j.tecto.2009.02.023.
Rumpker, G., and T. Ryberg (2000), New Fresnel-zone estimates for shear-wave splitting observations from finite-difference modeling, *Geophys. Res. Lett.*, *27*, 205–208.
Savage, M. K. (1999), Seismic anisotropy and mantle deformation: What have we learned from shear wave splitting?, *Rev. Geophys.*, *37*, 65–106.
Schilling, J.-G., R. Kingsley, B. Hanan, and B. McCully (1992), Nd-Sr-Pb isotopic variations along the Gulf of Aden: Evidence for the Afar mantle plume-lithosphere interaction, *J. Geophys. Res.*, *97*, 10,927–10,966.
Sicilia, D., et al. (2008), Upper mantle structure of shear-waves velocities and stratification of anisotropy in the Afar Hotspot region, *Tectonophysics*, *462*, 164–177.
Silver, P. G. (1996), Seismic anisotropy beneath the continents: Probing the depths of geology, *Annu. Rev. Earth Planet. Sci.*, *24*, 385–432.
Silver, P. G., and W. W. Chan (1991), Shear wave splitting and subcontinental mantle deformation, *J. Geophys. Res.*, *96*, 16,429–16,454.
Silver, P. G., and M. Savage (1994), The interpretation of shear-wave splitting parameters in the presence of two anisotropic layers, *Geophys. J. Int.*, *119*, 949–963.
Smith, W. H. F., and P. Wessel (1990), Gridding with continuous curvature splines in tension, *Geophysics*, *55*, 293–305.
Tommasi, A., D. Mainprice, P. Cordier, C. Thoraval, and H. Couvy (2004), Strain-induced seismic anisotropy of wadsleyite polycrystals and flow patterns in the mantle transition zone, *J. Geophys. Res.*, *109*, B12405, doi:10.1029/2004JB003158.
Vauchez, A., A. Tommasi, G. Barruol, and J. Maumus (2000), Upper mantle deformation and seismic anisotropy in continental rifts, *Phys. Chem. Earth*, *25*, 111–117.
Vinnik, L. P., V. Farra, and B. Romanowicz (1989), Azimuthal anisotropy in the Earth from observations of *SKS* at Geoscope and NARS broadband stations, *Bull. Seismol. Soc. Am.*, *79*, 1542–1558.
Walker, K. T., A. A. Nyblade, S. L. Klemperer, G. H. R. Bokelmann, and T. J. Owens (2004), On the relationship between extension and anisotropy: Constraints from shear wave splitting across the East African Plateau, *J. Geophys. Res.*, *109*, B08302, doi:10.1029/2003JB002866.
Walker, K. T., G. H. R. Bokelmann, S. L. Klemperer, and A. Nyblade (2005), Shear wave splitting around hotspots: Evidence for upwelling-related mantle flow?, *Spec. Pap. Geol. Soc. Am.*, *388*, 171–192, doi:10.1130/2005.2388(11).
Wolfe, C. J., F. L. Vernon, and A. Al-Amri (1999), Shear-wave splitting across western Saudi Arabia: The pattern of upper mantle anisotropy at a Proterozoic shield, *Geophys. Res. Lett.*, *26*, 779–782.
Wright, T., C. Ebinger, J. Biggs, A. Ayele, G. Yirgu, D. Keir, and A. Stork (2006), Magma-maintained rift segmentation at continental rupture in the 2005 Afar dyking episode, *Nature*, *442*, 291–294.
Zhang, S., and S. I. Karato (1995), Lattice preferred orientation of olivine aggregates deformed in simple shear, *Nature*, *375*, 774–777, doi:10.1038/375774a0.

M. G. Abdelsalam, S. S. Gao, and K. H. Liu, Department of Geological Sciences and Engineering, Missouri University of Science and Technology, Rolla, MO 65409, USA. (abdelsam@mst.edu; sgao@mst.edu; liukh@mst.edu)